Biosensors and Bioelectronics 127 (2019) 57–63

Contents lists available at ScienceDirect

Biosensors and Bioelectronics

journal homepage: www.elsevier.com/locate/bios

Molecularly imprinted photoelectrochemical sensor for fumonisin B_1 based on GO-CdS heterojunction

Lebao Mao[a,b], Kailun Ji[b], Linli Yao[b], Xiaojie Xue[b], Wei Wen[a,b], Xiuhua Zhang[a,b,*], Shengfu Wang[a,b]

[a] Hubei Collaborative Innovation Center for Advanced Organic Chemical Materials, Hubei University, Wuhan 430062, China
[b] Ministry-of-Education Key Laboratory for the Synthesis and Application of Organic Functional Molecules, College of Chemistry and Chemical Engineering, Hubei University, Wuhan 430062, China

ARTICLE INFO

Keywords:
Photoelectrochemical sensor
GO-CdS heterojunction
Molecularly imprinted polymer
Fumonisin B_1

ABSTRACT

A rapid and ultrasensitive molecularly imprinted photoelectrochemical (MIP-PEC) sensing platform based on ITO electrode modified with GO-CdS heterojunction was prepared for ultrasensitive measure of fumonisin B_1 (FB_1). CdS quantum dots (QDs) were combined with a suitable amount of graphene oxide (GO) to form a heterojunction to enhance signal response with accurately calculating energy levels (VB/CB or HOMO/LUMO). The MIP-PEC sensor was successful fabricated after MIP was immobilized on the electrode with the basis of these results. In the phosphate buffer solution (PBS), it was clearly observed that the non-elution MIP-PEC sensor had almost no photocurrent response, which was due to the slower electron transfer speed. When the MIP-PEC sensor is eluted in ethanol, its photocurrent response was significantly restored, that was because the fact that the template molecules were washed away, and electron donors entered the holes and accelerated the electron transfer. Its photocurrent response was reduced because of holes blocked when the MIP-PEC sensor was hatched in the template molecules culture fluid. This phenomenon fully showed that the MIP-PEC sensor can specifically detect the target. Thus, The work has a linear range from 0.01 to 1000 ng mL^{-1} with a detection limit of 4.7 pg mL^{-1} for FB_1. Furthermore, the fabricated MIP-PEC sensor will confirm the actual application.

1. Introduction

Fumonisins B_1 (FB_1) are mainly produced by Fusarium species that grows on agricultural commodities in the field or during storage, which are frequently associated with maize worldwide (Lukacs et al., 1996), but recently a widespread discovery of FB_1 had been found in other foods like beer, brewer grains, wine, rice, semolina, sorghum, millet or durum wheat pasta (Scott, 2012), so many diseases are attributed to FB_1 (Bartók et al., 2010; Smith et al., 2015). Thus, food safety and medical diagnosis required precise detection of FB_1. So far, many detection methods have been developed to measure FB_1, on the one hand, the traditional analytical methods of high performance liquid chromatography (HPLC) (Girolamo et al., 2010), thin-layer chromatography (TLC) (Rottinghaus et al., 1992) and liquid chromatography-mass spectrometry (LC-MS) (Gazzotti et al., 2009), but these methods require expensive instrumentation and trained personnel; on the other hand, some new analytical methods of enzyme-linked immunosorbent assay (ELISA) (Wang et al., 2014a, 2014b) and electrochemiluminescence (Zhang et al., 2017) because of their rapidity and sensitivity. In addition, there are a few novel ways to develop for FB_1 determination (Ezquerra et al., 2015; Chen et al., 2018). All above analytical methods developed have their advantages for FB_1 detection in real samples.

Since it was mentioned, photoelectrochemical (PEC) has been actively promoted, and now attracts a large number of research in various fields due to its notable advantages (Freeman et al., 2013). Essentially, this method of analysis, which is based on the principle of photoelectrochemistry, PEC has exactly the opposite detection procedure from electrochemiluminescence using an optical signal as an excitation source and detecting electrochemical signals, so it combines two features of optical analysis and electrochemical analysis (Zhao et al., 2016a, 2016b; Tanne et al., 2011; Li et al., 2015a, 2015b), exhibiting lower background but higher sensitivity than common electrochemical analysis apart from low cost, simple instrumentation and easy miniaturization (Tu et al., 2010; Li et al., 2015a, 2015b). Currently, photoelectrochemical (PEC) analysis technology shows its proves potential in chemical and biological analysis (Zhao et al., 2014a, 2014b; Li et al., 2017).

Molecular imprinting polymers (MIPs), it has been rapidly

* Corresponding author at: Hubei Collaborative Innovation Center for Advanced Organic Chemical Materials, Hubei University, Wuhan 430062, China.
E-mail address: zhangxh@hubu.edu.cn (X. Zhang).

https://doi.org/10.1016/j.bios.2018.11.040
Received 25 June 2018; Received in revised form 9 October 2018; Accepted 21 November 2018
Available online 06 December 2018
0956-5663/

developed and applied since it was proposed because of its high selectivity, chemical stability, low cost and easy preparation (Yang and Zhang, 2011) which is useful for preparing excellent performance sensors (Gam-Derouich et al., 2012; Yang et al., 2013; Prasad et al., 2013; Zhang et al., 2013). Many methods for preparing molecularly imprinted polymers have now been improved such as electrochemical polymerization (Wang et al., 2014a, 2014b), precipitation polymerization (Sambe et al., 2006), and so on. Thus, when molecular imprinting technology is introduced to PEC, the sensor selectivity will be greatly enhanced for specific molecular recognition, the development of photoelectrochemical sensor based on molecular imprinting technology will be welcomed by researchers.

To prepare a classic PEC detection system, different photoactive materials and biological receptors could influence the quality of the PEC sensor. Among them, the photoactive material formed the basis and it can affect the photoelectric conversion efficiency (Zhao et al., 2014a, 2014b). Among numerous semiconducting, quantum dot (QD)-based PEC sensing platform for chemical and biological detection are a hot topic because of their special optical and electronic properties of QDs (Smith et al., 2008; Parak et al., 2005). CdS QDs are widely used as visible photoactive materials for PEC sensor due to its narrow band gap (Yue et al., 2013), unfortunately, photogenerated electrons and holes of pure CdS QDs also have the high recombination rate accompanied with photocorrosion (Wang et al., 2014a, 2014b), but when CdS QDs and graphene oxide (GO) are combined to form a heterojunction which contributes to the photoinduced charge separation (Lu et al., 2014; Fu et al., 2013; Li et al., 2014a, 2014b), and the heterojunction is the foundation for the preparation of the PEC sensor.

In this research, we fabricated an original MIP-PEC sensing platform for ultrasensitive detection of FB_1 which had not been reported so far. The processes of the MIP-PEC sensor and response mechanism of FB_1 in the photoelectrochemical sensing were illustrated in Fig. 1. First, the ultrasonically mixed CdS QDs, GO and chitosan (CS) were covered by the clean indium tin oxide (ITO) electrode which had been cleaned. Next, the electrode was being dried at 60 °C for 2 h, and then cooled to room temperature. Then, the original solution of MIP was immobilized on the GO/CdS/CS/ITO electrode by UV polymerization, and the MIP-PEC sensor was successfully prepared. Finally, the MIP-PEC sensor was eluted with ethanol before the detection. Importantly, when the photoelectric material was illuminated, electrons on the highest occupied molecular orbital (HOMO) of GO would absorb photons and then transfer to the lowest unoccupied molecular orbital (LUMO) to form electron-hole pairs. Then the electrons can quickly transfer to the CdS QDs through the interface between CdS and GO; while electrons on the valence band (VB) would absorb photons of CdS QDs and then transfer to the conduction band (CB), this not only produced a strong photocurrent, but also it effectively separated the photogenerated electrons and holes (Xu et al., 2017). At the same time, the electron donor in the solution can provide electrons to the VB of CdS to trap holes through the cavities of the MIP membrane, thus forming a loop for photocurrent generation. The results showed that the MIP-PEC sensor was successfully prepared with excellent performance and it can be applied to the detection of FB_1 in real samples.

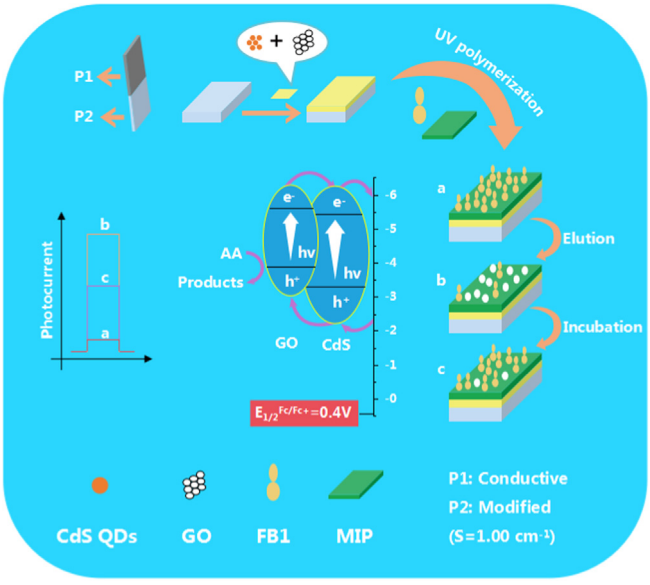

Fig. 1. Schematic illustration of the fabrication process of MIP-PEC sensor and the mechanism of photocurrent generation.

2. Materials and methods

2.1. Chemicals and reagents

Sodium sulfide nonahydrate ($Na_2S.9H_2O$), sodium hydroxide (NaOH), 3-mercaptopropionic acid ($C_3H_6O_2S$), cadmium chloride hemi (pentahydrate) ($CdCl_2.21/2H_2O$), triethanolamine (TEOA), ascorbic acid (AA), chitosan (CS), glucose (Glu) and starch were obtained from Aladdin Industrial Coperation (Shanghai. China). methacrylic acid (MAA), ethylene glycol dimethacrylate (EDMA), azodiisobutyronitrile (AIBN) were purchased from Sigma-Aldrich. Aqueous solution of graphene oxide was from sinocarbon-cas (GO, Shanxi China). Fumonisin B_1 (FB_1), ochratoxin A (OTA), ochratoxin B (OTB), deoxynivalenol (DON), Zearalenone (ZON) and Patulin (PAT) were bought from cayman chemical company (United States). And the maize meal and milk were purchased from the local supermarket. All other chemical reagents were of analytical grade, and millipore ultrapure water with a certain resistivity > 18.2 MΩ cm was used throughout the experiment. The working solution was using a homemade phosphate buffer solution (pH 7.4, KH_2PO_4-Na_2HPO_4, PBS) with 0.1 mol L^{-1} for MIP-PEC detection.

2.2. Apparatus

PEAC 200A PEC reaction instrument (Tianjin Aidahengsheng Science-Technology Development Co., Ltd., China). PEC signals were carried out by CHI660C electrochemical workstation (Shanghai Chenhua Apparatus Corporation, China) with a three-electrode system, and Indium tin oxide (10 × 45 × 1 mm) (South China Science & Technology Co., Ltd., China), platinum wire, and saturated Ag/AgCl were served as working electrode, counter electrode, and reference electrode, respectively. High speed freezing centrifuge (Beijing BMH Instruments Co. Ltd., shanghai, China). X-ray photoelectron spectroscopy (XPS) measurements were performed on an JSM6510LV instrument (Jeol, Japan), Scanning electron micrographs (SEM) were measured on a JEOL JSM7100F scanning electron microscope (Jeol, Japan), Transmission electron microscopy (TEM) images were employed to HITACHI H-7000FA transmission electron microscope at an acceleration voltage of 100 kV. The UV–vis spectra were obtained in a Shimadzu UV-2700 spectrometer and the fluorescence spectra were obtained from Shimadzu RF-5301pc spectrometer. UV polymerization was achieveed by ZF-I UV analyzer (Shanghai Guanghao Analysis Instrument Co., Ltd., shanghai, China).

2.3. Synthesis of CdS QDs

CdS QDs were prepared by a hydrothermal method with a slight change (Liu et al., 2015). Firstly, 10 mL of 0.02 M $CdCl_2.21/2H_2O$ was added into a beaker, and 2.0 M NaOH was used to adjust the pH of the solution to 10 after adding 15 μL of 3-mercaptopropionic acid, which became turbid from clear to clarify. Secondly, the mixed solution was moved to a 50 mL three-necked flask and heated to boiling under a nitrogen atmosphere. The next step, 10 mL of 0.02 M Na_2S solution was furtherly injected into the flask by an injector after 30 min, and the

reaction is maintained for 4 h under reflux. Finally, the cooled of stock solution was centrifuged at 9000 rpm for 10 min, it was washed several times with ethanol before vacuum drying. And CdS QDs could be dispersed by water for further use.

2.4. Preparation MIP-PEC and non-MIP (NIP)-PEC sensing platform

Firstly, the ITO electrode surface cleaned with a sequential employing acetone, ethanol, and ultrapure water by ultrasonic treatment for 30 min and then dried it. Next, the CdS QDs and 1 wt% chitosan were added into the aqueous solution of graphene oxide which had been sonicated for 10 min, and the mixture solution continued to sonic for 10 min. Subsequently, the ITO surface (modified area of 1.00 cm^2) was coated with 100 μL of GO/CdS/CS (GO accounted for 5%) mixed solution, and dried at 60 °C for 2 h. Then, the original solution of MIP included FB_1, MAA, EDMA and AIBN (MAA:EDMA:AIBN = 8:3:1), and 20 μL of the original solution was dropped on modified area with volume ratio was 2: 1. In the end, the MIP-PEC sensor was acquired by ultraviolet initiated polymerization for 10 min. As a control, the NIP-PEC sensor was prepared in the same way except the template molecules. The MIP-PEC and NIP-PEC sensors were eluted with ethanol for 20 min for further detection.

2.5. Photoelectrochemical measurement

The proposed MIP-PEC sensor was thoroughly cleaned with ultrapure water and then incubated in FB_1 solution for 15 min. The photocurrent responses were measured in PBS solution (0.1 M, pH = 7.4) containing 0.04 M AA as a sacrificial electron donor with a three-electrode system illuminated by 455 nm light. The light was switched on 20 s and off 10 s in turn, and the applied potential was + 0.5 V.

3. Results and discussion

3.1. Characterization of MIP-PEC sensing platform

The morphology and particle sizes of the prepared CdS QDs and imprinted film were characterized by TEM, XPS and SEM (Fig. 2). From Fig. 2A, CdS QDs exhibited as quasi-spherical particles with average sizes at about 4 nm. To further confirm the successful preparedness of CdS, the XPS measurements were used to show the chemical composition and chemical state of constituent elements. There were the elements of Cd, S, C and O in the XPS survey spectrum (Fig. 2B). The photoelectron peaks at 405.1 eV and 411.9 eV, and the peaks at 161.1 eV and 162.2 eV are assigned to Cd $3d_{5/2}$, Cd $3d_{3/2}$, S $2p_{3/2}$, and S $2p_{1/2}$(Lu et al., 2014; Zhang et al., 2014), respectively. The small amount of C 1s and O 1s were caused to the use of $C_3H_6O_2S$ as a stabilizer during the synthesis. Thus, these XPS results further confirm the successful formation of CdS QDs. Meanwhile, the UV–vis and FL spectrums of CdS QDs, GO and GO-CdS were presented in Fig. S1, respectively. CdS QDs has an absorption at the range of 300–550 nm, GO has an absorption at the range of 300–800 nm, and they all have a good absorption and emission indicating the potential for efficient photoelectric conversion in the visible range.

As can be seen from the Fig. 2C and D, When NIP and MIP were compared, on the on hand, they all indicated that the imprinted polymer film were successfully prepared; on the other hand, NIP and MIP could not be identified and distinguished by SEM due to the size of molecular.

3.2. EIS characterization of the MIP-PEC sensor fabrication

The capability of electron transfer of the electrodes modified with different materials was investigated by EIS. As showed in Fig. 3A, the resistance of ITO electrode (curve a) was smallest,when GO/CdS/CS was modified on ITO electrode, the GO/CdS/CS/ITO electrode (curve b) would hinder the electron transfer, simultaneously, the impedance does not increase much because it had a certain conductivity. The MIP was coated on the modified electrode while the resistance electrode (curve c) was obviously increased thanks to the high density of the insulation imprinted membrane. It also could be seen that the resistance decreased rapidly after the FB_1 were eluted (curve d), indicating that more electron transfer channels were formed to increase the contact area between the electron donor and the sensor and accelerate electron transfer. Ideally, there was a few increase here compared to elution after template incubated (curve e) because the cavity was refilled by the template molecule, but it could not match the one before the elution, and R_{et} were 39 Ω, 232 Ω, 16610 Ω, 4642 Ω and 10380 Ω based on the Randle's model equivalent circuit, respectively. All the EIS results showed the successful prepare of MIP-PEC sensing platform and it also could specifically recognize FB_1.

3.3. Calculation of HOMO/LUMO or VB/CB energy levels of materials

The electrochemical properties of these materials were further investigated by CV with the results displayed in Fig. 3B. Mostly, The band diagrams of CB and VB in early reports recieved by calculations, which based on their bulk electron affinity (EA) and ionization potential (IP) (Dissanayake et al., 2008) by using the following equations: IP = -(4.80 - $E_{1/2}^{Fc/Fc+}$ + E_{ox}), EA = IP + Eg; Eg = 1240/λ_{onset} (Li et al., 2014a, 2014b), Similarly, the equations: E_{HOMO} = -(4.80 - $E_{1/2}^{Fc/Fc+}$ + E_{ox}), E_{LUMO} = E_{HOMO} + E_g can deduced the energy levels of LUMO and HOMO of polymer ($E_{1/2}^{Fc/Fc+}$ is the formal potential of Fc/Fc^+, E_{ox} is the oxidation initiation potential, and E_g is optical band gap, λ_{onset} was first exciton absorption peak) (Hou et al., 2006). And under the premise that the energy level of Fc/Fc^+ was 4.8 eV below the vacuum level (Pommerehne et al., 1995). As can be seen, the E_{ox} of CdS QDs and GO were disclosed as 1.40 V and 1.51 V. From Fig. 3B inset, $E_{1/2}^{Fc/Fc+}$ was measured as + 0.40 V, and 551 nm and 796 nm were determined as the λ_{onset} of CdS QDs and GO (Fig. S1A), corresponding to Eg of 2.25 eV and1.56 eV, respectively. Using the equations, the CB/VB or LUMO/HOMO of materials was calculated as −3.55 eV/-5.80 eV and −4.35 eV/-5.91 eV in Table S1 in Supporting information, respectively. These information would be important for explaining the PEC responses of the prepared heterojunction.

3.4. Optimization of electron donor

It is a known fact that suitable electron donors and acceptors can convert specific sensing events into corresponding current signals in a typical PEC sensing mechanism. Although heterojunction have been formed, if there are no electron donors in the solution to trap holes, then the hole will react with the S^{2-} of CdS itself as follows: $2h^{2+}$ + CdS→ Cd^{2+} + S, resulting in photocorrosion of CdS QDs. Na_2S, TEOA, and AA as electron donors are selected here (Fig. S2). As can be seen, compared with PBS buffer solution, All three kinds of donors can increase the photocurrent, and the enhanced effect of AA is better than Na_2S and TEOA, Therefore, AA is selected as an electron donor throughout the experiment.

The concentration of AA was optimized to achieve the satisfactory photocurrent response signal. The photocurrent response signal was progressively enhanced with the increase of the concentration of AA because it could capture holes more quickly. When it reaches 0.04 M, the signal reaches the highest point, and the concentration of ascorbic acid increased again, the photocurrent signal gradually became smaller likely resulted from the quenching effect of high AA concentrations on photocurrent. Therefore, 0.04 M was picked as the optimal concentration of electron donor.

3.5. PEC response of MIP-PEC sensor

The photoelectric conversion properties of material modified ITO

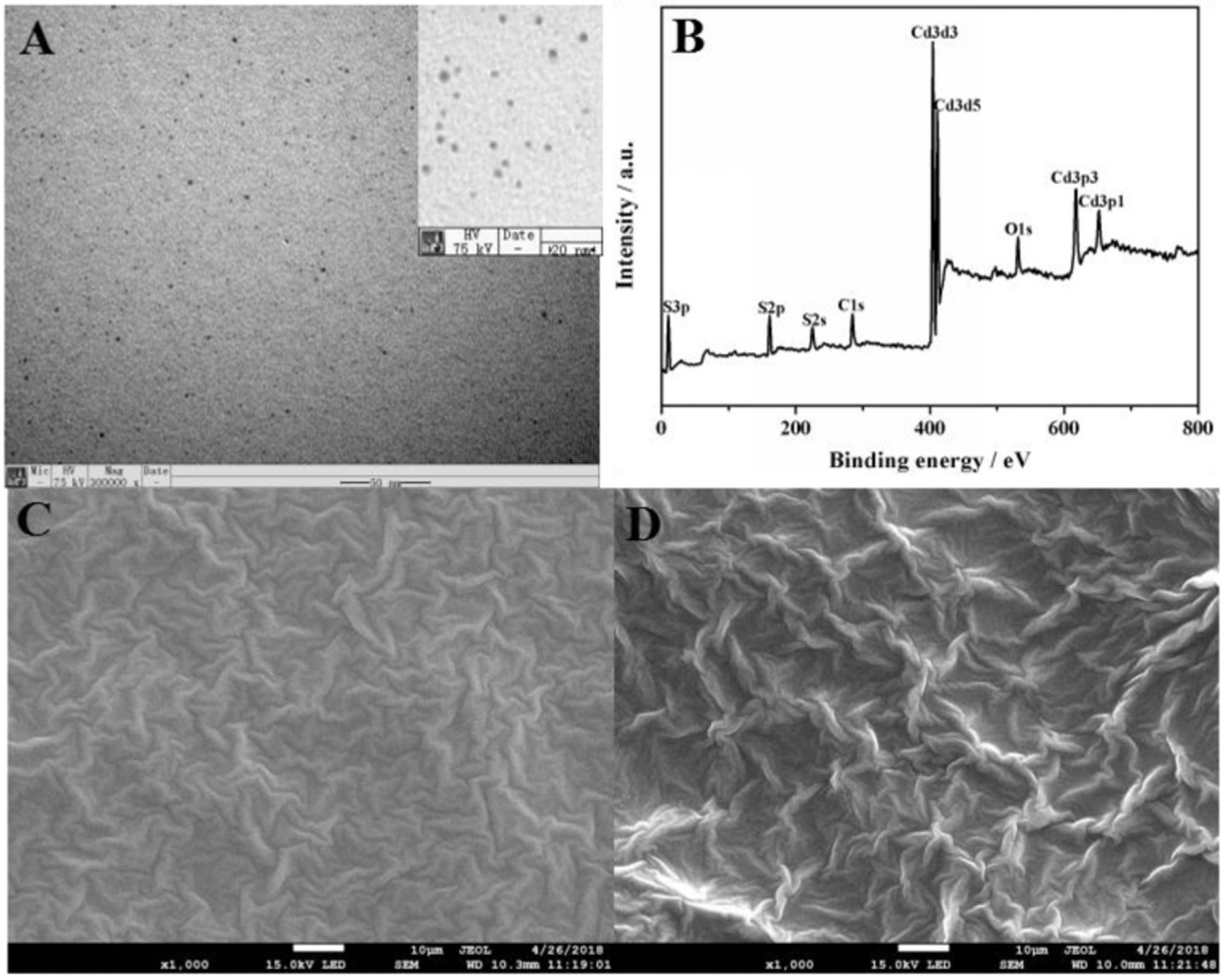

Fig. 2. (A) TEM images of CdS QDs; (B) XPS survey spectrum of CdS QDs; (C) SEM images of NIP/GO/CdS/CS/ITO; (D) MIP/GO/CdS/CS/ITO.

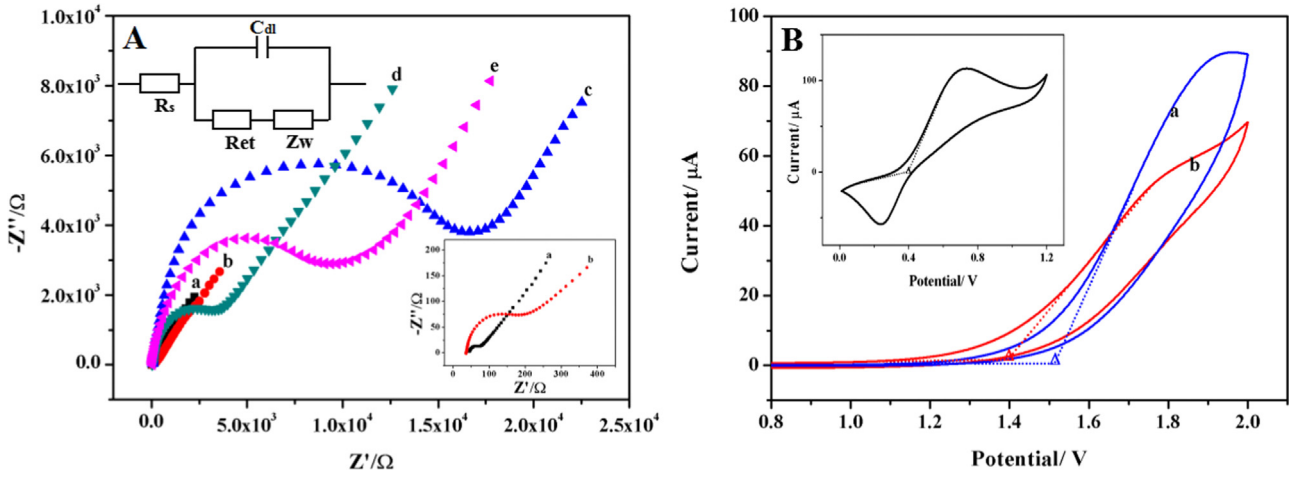

Fig. 3. (A) EIS in 0.1 M KCl solution containing 5.0 mM $[Fe(CN)_6]^{3-/4-}$. (a) ITO; (b) GO/CdS/CS/ITO; (c) MIP/GO/CdS/CS/ITO before template eluted; (d) MIP/GO/CdS/CS/ITO after template eluted; (e) MIP/GO/CdS/CS/ITO after template incubated. Insets: the Randle's model equivalent circuit and the partial enlargement of (a) and (b). Potential: 0.208 V, frequency range: 10 mHz to 100 kHz. (B) CVs of the ITO modified by (a) GO and (b) CdS in deoxygenated anhydrous acetonitrile solution of tetrabutylammonium hexafluorophosphate (0.1 M); E_{ox} were calculated from tangents of species oxidation peaks. Insets: CVs of the ITO (as working electrodes) in a deoxygenated anhydrous acetonitrile solution of tetrabutylammonium hexafluorophosphate (0.1 M) and ferrocene (0.5 mM) at scan rate of 50 mV s^{-1}, with a Pt wire counter electrode, an Ag/AgCl reference electrode (with saturated KCl).

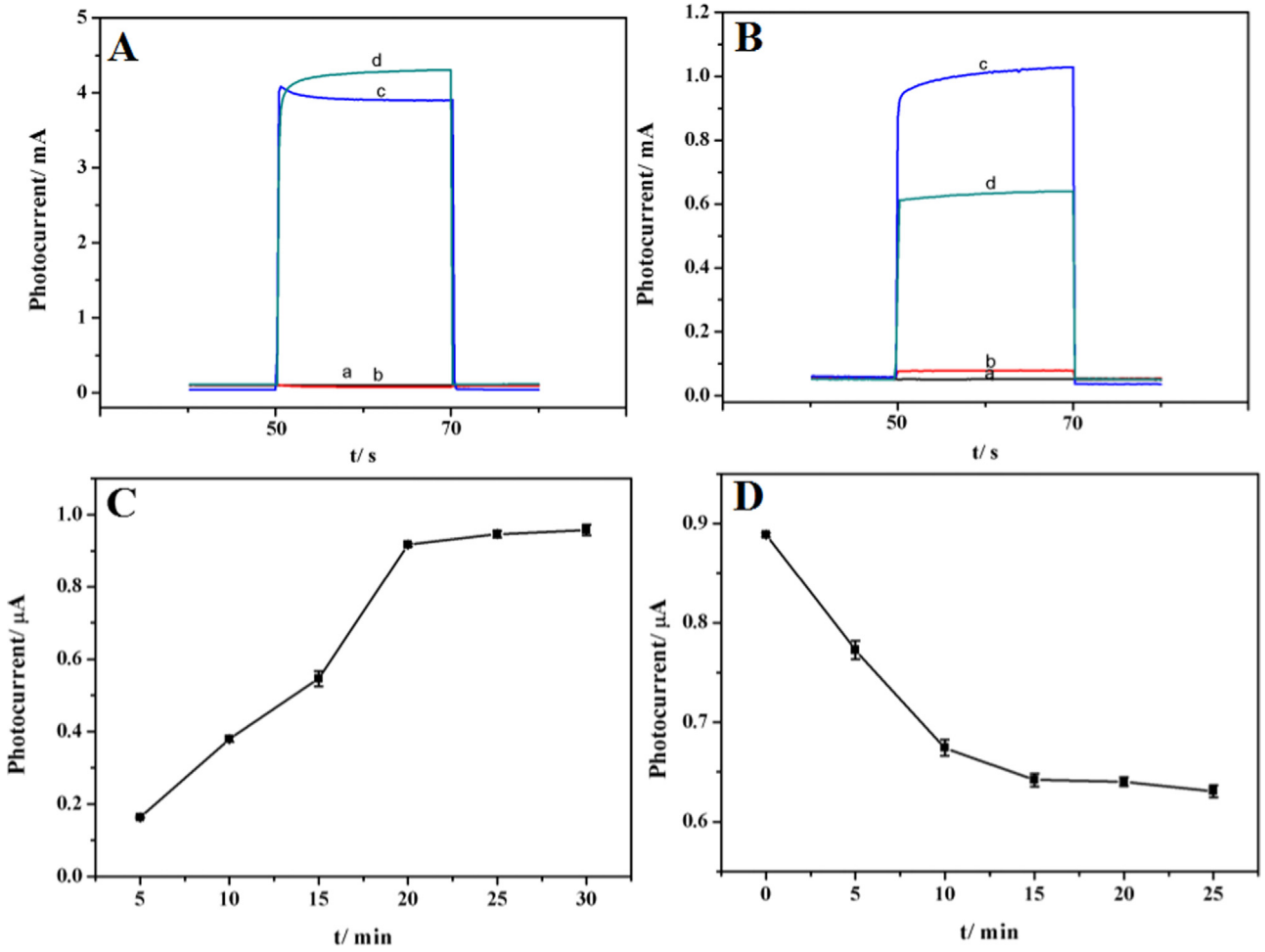

Fig. 4. (A) Photocurrent responses of (a) ITO; (b) GO/CS/ITO; (c) CdS/CS/ITO; (d) GO/CdS/CS/ITO. (B) Photocurrent responses of (a) ITO; (b) MIP/GO/CdS/CS/ITO before template eluted; (c) MIP/GO/CdS/CS/ITO after template eluted; (d) MIP/GO/CdS/CS/ITO after template incubated. (C) Effect of the duration of elution. (D) Effect of the duration of incubation.

electrode were evaluated, the photocurrent responses of GO/CS-, CdS/CS-, GO/CdS/CS- and MIP/GO/CdS/CS- modified ITO electrodes were recorded under PEC measurement equipped with light source (Fig. 4A). From the figure, the bare ITO electrode did not have a photocurrent response (curve a), but the GO/CS/ITO electrode showed a low cathode photocurrent response (curve b). When the electrode is modified by CdS QDs, it could be clearly observed that the anode photocurrent response was very large without stable photocurrent (curve c), which was due to the narrow band gap of the CdS QDs and photocorrosion (Zhong et al., 2003). After compounding GO with CdS QDs, photocurrent was enhanced and stabilized (curve d), this was due to the formation of nanocomposites reduced the recombination rate of electron-hole pairs to produce a stable photocurrent (Lu et al., 2014; Fu et al., 2013; Li et al., 2014a, 2014b), but it had not been greatly enhanced because of the poor electrical conductivity of GO. By comparison, a good photocurrent response provided a way to develop PEC sensors.

Compared with the GO/CdS/CS/ITO electrode, it can be clearly seen that the non-elution MIP-PEC sensor had almost no photocurrent response, which was not much different from the bare electrode in Fig. 4B (curve a and b). When the MIP-PEC sensor is eluted in ethanol, its photocurrent response was significantly restored (curve c), which was based on the fact that FB_1 were washed away, and electron donors entered the caves and accelerated the electron transfer. Its photocurrent response was reduced owing to holes blocked after incubating in the template molecules solution (curve d). It also could be seen the photocurrent response of the NIP-PEC sensor in Fig. S3., there was no change between elution and incubation. This phenomenon fully showed that the MIP-PEC sensor can specifically detect the target.

3.6. Optimization of elution and incubation time

The MIP-PEC electrode was eluted with ethanol as showed in Fig. 4C. The photocurrent increased requiring longer elution time, and the photocurrent remained almost unchanged after 20 min of elution, which proved that most FB_1 had been removed from the surface of MIP film. Thus, 20 min was the optimal duration of elution. It could be found from Fig. 4D after incubation, the photocurrent response apparently decreased accompanied with the growth of incubation time in 1.0 ng mL^{-1} FB_1, and the photocurrent remained almost stable after 15 min of incubation, indicating the template molecules had reached equilibrium. In consequence, 15 min was selected to be the optimal duration of incubation.

3.7. Analytical performance of the MIP-PEC assay

The developed MIP-PEC sensor was served for FB_1 detection under optimal experimental conditions. The PEC responses of the sensor toward different concentrations of FB_1 for detection. A higher response was obtained without FB_1 while the photocurrent response decreased with the mounting concentrations of FB_1 from a to g (0–1000 ng mL^{-1}), meaning that more caves were filled (Fig. 5A). Furthermore, the MIP-PEC response was found that the photocurrent was a negative

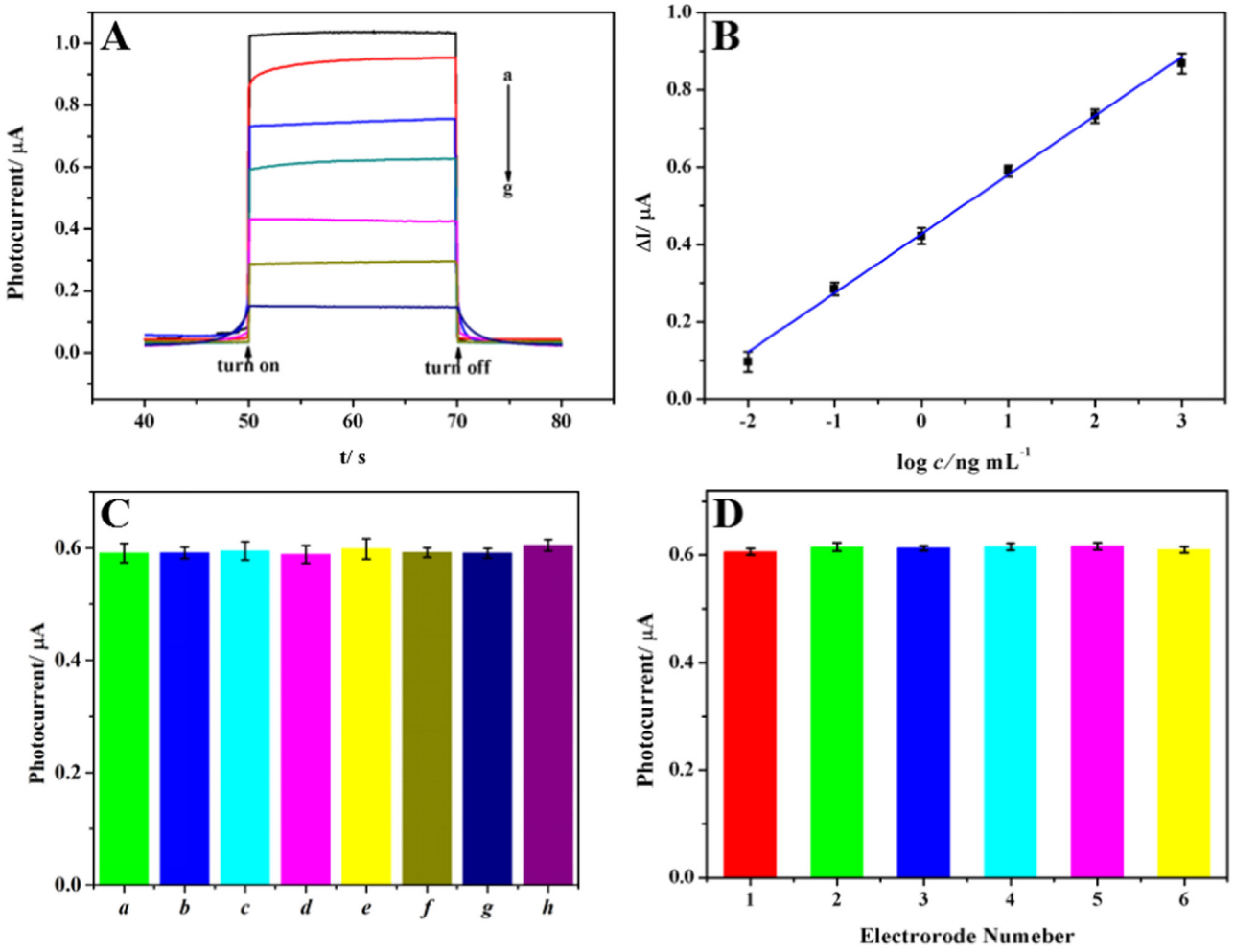

Fig. 5. (A) Photocurrent responses of MIP-PEC sensor in different concentrations of FB_1. (B) the calibration curve of FB_1 determination. (C) Selectivity of the proposed MIP-PEC sensor: the mixture (containing 10 ng mL^{-1} of OTA, 10 ng mL^{-1} of OTB, 10 ng mL^{-1} of DON, 10 ng mL^{-1} of ZON, 10 ng mL^{-1} of PAT, 10 ng mL^{-1} of Glu, 10 ng mL^{-1} of Starch and 1.0 ng mL^{-1} of FB_1) and FB_1 (1.0 ng mL^{-1}), which were replaced by a, b, c, d, e, f, g, and h. (D) Reproducibility of the MIP-PEC sensor with six electrodes in 1.0 ng mL^{-1} of FB_1.

correlation to the logarithmic value of FB_1 concentration (Fig. 5B). The linear regression equation was $\Delta I = 0.153 \log (c, \text{ ng mL}^{-1}) + 0.428$ (correlation coefficient $R^2 = 0.997$). According to the method of $LOD = 3S_B/m$ (Radi et al., 2006), the limit of detection (LOD) was estimated as 4.7 pg mL^{-1}, this MIP-PEC sensor showed a wider linear range with a lower detection limit, which was lower than those of previously reported FB_1 detection methods (Table S2).

3.8. Selectivity, reproducibility and stability of the fabricated MIP-PEC platform

Toxins associated with fumonisins might interfere with sample detection. Common interference was selected as interference conditions to evaluate the selectivity photoelectrochemical MIP-PEC sensor. As can be seen in Fig. 5C, changes in the PEC signal obtained from the mixtures were no obvious difference when compared with that of FB_1 apart from individual interference because the caves in the surface of MIP could distinguish FB_1 from other molecules, showing an excellent selectivity and specificity of the MIP-PEC sensor. Furthermore, the prepared MIP-PEC sensors could be used to detect real samples.

Generally, the reproducibility of the sensor was one of the keys to its practical application. The MIP-PEC sensor photocurrent responses were chronicled in six different electrodes after the incubation of 1.0 ng mL^{-1} FB_1. It can be observed from Fig. 5D, there was no difference in photocurrent response of six electrodes, and the relative standard deviation RSD was about 1.2%, it was equipped with an excellent reproducibility.

Stability was also a factor in evaluating the merits of MIP-PEC sensors. The photocurrent responses were recorded under 15 on/off irradiation cycles after incubating in 100 ng mL^{-1} FB_1. It exhibited a stable photocurrent response with a RSD of 3.0% (Fig. S4), which proved that the prepared sensor could be repeatedly.

3.9. Real samples analysis

FB_1 was processed in milk and maize samples following the reporting method (Zhang et al., 2017). And the recovery experiment was carried out with three different concentrations of standard FB_1 solution.

Table 1
Detection of FB_1 in real samples by the MIP-PEC sensor.

Sample name		Added (ng mL^{-1})	Found (ng mL^{-1})	Recovery (%)	RSD (n = 3) (%)
maize	1	0.1	0.09403	94.03	1.3
	2	1	1.0641	106.41	2.1
	3	10	10.2969	102.97	3.7
milk	1	0.1	0.09547	95.47	1.6
	2	1	1.0581	105.81	3.5
	3	10	9.4612	94.61	2.0

As showed in Table 1, the recovery rate of MIP-PEC sensor ranged from 94.03% to 106.41%, with the RSD between 1.3% and 3.7%, which indicated that the prepared sensor equipped with a good detection effect for FB_1 in the real samples.

4. Conclusions

In brief, a novel GO-CdS heterojunction-based MIP-PEC sensor had been successfully developed for FB_1 determination. It combined theoretical calculations, molecular imprinting technology and photoelectrochemistry. As a result, this approach showed an outstanding analytical performance with excellent selectivity, stability, reproducibility as well as an enhanced photocurrent based a heterojunction by accurately calculating energy levels (VB/CB or HOMO/LUMO). Importantly, the preparing of molecularly imprinted photoelectrochemical sensor for FB_1 determination had not been reported so far. Meanwhile, this method showed a wider linear range form 0.01–1000 ng mL^{-1} with a lower detection limit as 4.7 pg mL^{-1}. Fortunately, molecular imprinted photoelectrochemical sensor can be extended to real sample detection of FB1 and provide ideas for detection of additional substances in future work.

Acknowledgements

This work was financially supported by the National Natural Science Foundation of China (Nos. 11674085 and 21375033), the Natural Science Foundation of Hubei Province (Nos. 2011CDA111 and 2014CFA015), and National College Students' Innovation and Entrepreneurship Training Programs (No. 201610512044).

Appendix A. Supporting information

Supplementary data associated with this article can be found in the online version at doi:10.1016/j.bios.2018.11.040.

References

Bartók, T., Tölgyesi, L., Szekeres, A., Varga, M., Bartha, R., Szécsi, Á., Bartók, M., Mesterha´zy, Á., 2010. Rapid Commun. Mass Spectrom. 24, 35–42.
Chen, X.R., Liang, Y., Zhang, W.J., Leng, Y.K., Xiong, Y.H., 2018. Talanta 186, 29–35.
Dissanayake, D.M.N.M., Lutz, T., Curry, R.J., Silva, S.R.P., 2008. Appl. Phys. Lett. 93, 138.
Ezquerra, A., Vidal, J.C., Bonel, L., Castillo, J.R., 2015. Anal. Methods 7, 3742–3749.
Fu, J., Chang, B.B., Tian, Y.L., Xi, F.N., Dong, X.P., 2013. J. Mater. Chem. A 1, 3083–3090.
Freeman, R., Girsh, J., Willner, I., 2013. ACS Appl. Mater. Interfaces 5, 2815.
Gam-Derouich, S., Jouini, M., Hassen-Chehimi, D.B., Chehimi, M.M., 2012. Electrochim. Acta 73, 45–52.
Gazzotti, T., Lugoboni, B., Zironi, E., Barbarossa, A., Serraino, A., Pagliuca, G., 2009. Food Control. 20, 1171–1174.
Girolamo, A.D., Pereboomde Fauw, D., Sizoo, E., Egmond, H.P.V., Gambacorta, L., Bouten, K., Stroka, J., Visconti, A., Solfrizzo, M., 2010. World Mycotoxin J. 3, 135–146.
Hou, J.H., Tan, Z.A., Yan, Y., He, Y.J., Yang, C.H., Li, Y.F., 2006. J. Am. Chem. Soc. 128, 4911–4916.
Li, R.Z., Liu, Y., Cheng, L., Yang, C.Z., Zhang, J.D., 2014a. Anal. Chem. 8619, 9372–9375.
Li, S.G., Yuan, Z.C., Deng, P., Sun, B.B., Zhang, Q., 2014b. J. Mater. Chem. A 5, 2561–2566.
Li, R.Y., Zhang, Y., Tu, W.W., Dai, Z.H., 2017. ACS Appl. Mater. Interfaces 9.
Li, C.X., Wang, H.Y., Shen, J., Tang, B., 2015a. Anal. Chem. 87, 4283–4291.
Li, Z.Z., Xin, Y.M., Zhang, Z.H., 2015b. Anal. Chem. 87, 10491–10497.
Liu, Y., Yan, K., Zhang, J.D., 2015. ACS Appl. Mater. Interfaces 8, 28255.
Lukacs, Z., Schaper, S., Herderich, M., Schreier, P., Humpf, H.U., 1996. Chromatographia 43, 124–128.
Lu, M.L., Pei, Z.X., Weng, S.X., Feng, W.H., Fang, Z.B., Zheng, Z.Y., Huang, M.L., Liu, P., 2014. Phys. Chem. Chem. Phys. 16, 21280–21288.
Parak, W.J., Pellegrino, T., Plank, C., 2005. Nat. Nanotechnol. 16, R9.
Pommerehne, J., Vestweber, H., Guss, W., Mahrt, R.F., Bässler, H.M., Porsch, M., Daub, J., 1995. Adv. Mater. 7, 551–554.
Prasad, B.B., Prasad, A., Tiwari, M.P., 2013. Electrochim. Acta 102, 400–408.
Radi, A.E., Acero Sánchez, J.L.A., Baldrich, E., O'Sullivan, C.K., 2006. J. Am. Chem. Soc. 128, 117–124.
Rottinghaus, G.E., Coatney, C.E., Minor, H.C., 1992. J. Vet. Diagn. Invest. 4, 326–329.
Sambe, H., Hoshina, K., Moaddel, R., Wainer, I.W., Haginaka, J., 2006. J. Chromatogr. A 1134, 88–94.
Scott, P.M., 2012. Food Addit. Contam. A 29, 242.
Smith, A.M., Duan, H., Mohs, A.M., Nie, S., 2008. Adv. Drug Deliv. Rev. 60, 1226–1240.
Smith, A.M., Marbella, L.E., Johnston, K.A., Hartmann, M.J., Crawford, S.E., Kozycz, L.M., Seferos, D.S., Millstone, J.E., 2015. Anal. Chem. 87, 2771–2778.
Tanne, J., Schafer, D., Khalid, W., Parak, W.J., Lisdat, F., 2011. Anal. Chem. 83, 7778–7785.
Tu, W.W., Dong, Y.T., Lei, J.P., Ju, H.X., 2010. Anal. Chem. 82, 8711–8716.
Wang, R., Yan, K., Wang, F., Zhang, J.D., 2014a. Electrochim. Acta 121, 102–108.
Wang, Y.K., Wang, Y.C., Wang, H.A., Ji, W.H., Sun, J.H., Yan, Y.X., 2014b. Food Control. 40, 41–45.
Xu, L., Ling, S.Y., Li, H.N., Yan, P.C., Xia, J.X., Qiu, J.X., Wang, K., Li, H.M., Yuan, S.Q., 2017. Sens. Actuators B 240, 308–314.
Yang, Y.K., Fang, G.Z., Liu, G.Y., Pan, M.F., Wang, X.M., Kong, L.J., He, X.L., Wang, S., 2013. Biosens. Bioelectron. 47, 475–481.
Yang, Z.P., Zhang, C.J., 2011. Biosens. Bioelectron. 29, 167–171.
Yue, Z., Lisdat, F., Parak, W.J., Hickey, S.G., Tu, L.P., Sabir, N., Dorfs, D., Bigall, N.C., 2013. ACS Appl. Mater. Interfaces 5, 2800–2814.
Zhang, J., Lei, J.P., Ju, H.X., Wang, C.Y., 2013. Anal. Chim. Acta 786, 16–21.
Zhang, L.J., Zheng, R., Li, S., Liu, B.K., Wang, D.J., Wang, L.L., Xie, T., F., 2014. ACS Appl. Mater. Interfaces 6, 13406–13412.
Zhang, W., Xiong, H.W., Chen, M.M., Zhang, X.H., Wang, S.F., 2017. Biosens. Bioelectron. 96, 55.
Zhao, W.W., Xu, J.J., Chen, H.Y., 2014a. Chem. Rev. 114, 7421–7441.
Zhao, Y., Luo, Y.D., Li, T.T., Song, Q.J., 2014b. RSC Adv. 4, 57709–57714.
Zhao, W.W., Xu, J.J., Chen, H.Y., 2016a. Analyst 141, 4262–4271.
Zhao, W.W., Xu, J.J., Chen, H.Y., 2016b. Biosens. Bioelectron. 92, 294.
Zhong, X.H., Feng, Y.Y., Knoll, W., Han, M.Y., 2003. J. Am. Chem. Soc. 125, 13559.